



**HAL**  
open science

## Excited-State Reactivity of $[\text{Mn}(\text{im})(\text{CO})_3(\text{phen})]^+$ : A Structural Exploration

Maria Fumanal, Yu Harabuchi, Etienne Gindensperger, Satoshi Maeda,  
Chantal Daniel

► **To cite this version:**

Maria Fumanal, Yu Harabuchi, Etienne Gindensperger, Satoshi Maeda, Chantal Daniel. Excited-State Reactivity of  $[\text{Mn}(\text{im})(\text{CO})_3(\text{phen})]^+$  : A Structural Exploration. *Journal of Computational Chemistry*, 2019, 40 (1), pp.72-81. 10.1002/jcc.25535 . hal-02399602

**HAL Id: hal-02399602**

**<https://hal.science/hal-02399602>**

Submitted on 9 Dec 2019

**HAL** is a multi-disciplinary open access archive for the deposit and dissemination of scientific research documents, whether they are published or not. The documents may come from teaching and research institutions in France or abroad, or from public or private research centers.

L'archive ouverte pluridisciplinaire **HAL**, est destinée au dépôt et à la diffusion de documents scientifiques de niveau recherche, publiés ou non, émanant des établissements d'enseignement et de recherche français ou étrangers, des laboratoires publics ou privés.

# Excited-State Reactivity of $[\text{Mn}(\text{im})(\text{CO})_3(\text{phen})]^+$ : A Structural Exploration

Maria Fumanal,<sup>[a]</sup> Harabuchi Yu,<sup>[b,c]</sup> Etienne Gindensperger,<sup>[a]</sup> Satoshi Maeda<sup>[b,c]</sup> and Chantal Daniel<sup>[a]</sup>

The electronic excited states reactivity of  $[\text{Mn}(\text{im})(\text{CO})_3(\text{phen})]^+$  (phen = 1,10-phenanthroline; im = imidazole) ranging between 420 and 330 nm have been analyzed by means of relativistic spin-orbit time-dependent density functional theory and wavefunction approaches (state-average-complete-active-space self-consistent-field/multistate CAS second-order perturbation theory). Minimum energy conical intersection (MECI) structures and connecting pathways were explored using the artificial force induced reaction (AFIR) method. MECIs between the first and second singlet excited states ( $S_1/S_2$ -MECIs) were searched by the single-component AFIR (SC-AFIR) algorithm combined

with the gradient projection type optimizer. The structural, electronic, and excited states properties of  $[\text{Mn}(\text{im})(\text{CO})_3(\text{phen})]^+$  are compared to those of the Re(I) analogue  $[\text{Re}(\text{im})(\text{CO})_3(\text{phen})]^+$ . The high density of excited states and the presence of low-lying metal-centered states that characterize the Mn complex add complexity to the photophysics and open various dissociative channels for both the CO and imidazole ligands. © 2018 Wiley Periodicals, Inc.

DOI:10.1002/jcc.25535

## Introduction

Recent renewal of interest for transition metal carbonyls complexes has been motivated by the development of air-stable photo-activated carbon monoxide releasing moieties (photo-CORMs) labilized by visible light for biological applications.<sup>[1]</sup> This domain of research is very stimulating because of the demanded chemical, photochemical, and biological properties in a single molecule. Indeed, the potential photoCORMs  $\text{ML}_n(\text{CO})_m$  ( $M = \text{Fe}, \text{Ru}, \text{Cr}, \text{Mo}, \text{W}, \text{Mn}, \text{Co}, \text{Ir}$ ) should be stable and nontoxic in absence of light and in presence of water, oxygen, and other biological constituents. The complex should absorb at long wavelengths (visible, near-IR) to fit with the tissue penetration spectral domain. Therapeutic metal carbonyl complexes have received significant attention recently as suitable molecular vehicles for CO release under physiological conditions.<sup>[2]</sup> The advantage of the so-called photoCORMs prodrugs is that they can be distributed in the body as dark-stable inert molecules and be eventually activated by means of light for targeted function.

Transition metal carbonyl complexes containing  $\alpha$ -diimine ligands, such as bpy or phen (bpy = 2,2'-bipyridine; phen = 1,10-phenanthroline) are good candidates given their intense metal-to-ligand-charge-transfer (MLCT) absorption bands in the UV-visible. Knowing the essential role of manganese in biological processes a number of studies has been dedicated to  $[\text{Mn}(\text{CO})_3(\text{bpy}/\text{phen})(\text{L})]^{0/+}$  complexes. The photo-reactivity of this class of first-row transition metal complexes on irradiation in the visible has been associated to the presence of low-lying metal-centered (MC) states in the vicinity of the MLCT absorbing states.<sup>[3-7]</sup> Whereas extensive work, both experimental and theoretical, has been achieved on third-row analogues to understand and interpret the spectroscopy and the photophysics of the usually nonreactive  $[\text{Re}(\text{CO})_3(\text{bpy}/\text{phen})(\text{L})]^{0/+}$  compounds,<sup>[8-19]</sup> little is known on the optical and photophysical properties of  $[\text{Mn}(\text{CO})_3(\text{bpy}/\text{phen})(\text{L})]^{0/+}$  complexes.

While UV-visible irradiation of  $[\text{Re}(\text{im})(\text{CO})_3(\text{phen})]^+$  (im = imidazole) complex results in an ultrafast luminescent decay within a few hundred of fs<sup>[8]</sup> the irradiation of *fac*- $[\text{Mn}(\text{im})(\text{CO})_3(\text{phen})]^+$  (Scheme 1) leads to a very efficient *fac-to-mer* photo-isomerization in solution.<sup>[20-22]</sup> The absorbing state was ascribed to a low-lying MLCT transition while the reaction presumably occurs through a spectroscopically dark MC state. This is reminiscent to the conclusion of quantum dynamics simulations performed on  $[\text{Cr}(\text{CO})_4(\text{bpy})]$  where it is shown that after getting trapped into the potential wells of two low-lying MLCT states at Franck-Condon (FC), 10% of the system dissociates toward the axial CO loss in <500 fs via a potential that acquires MC character along this coordinate.<sup>[4]</sup>

The goals of this study are (1) to compare the structural, electronic, and excited states properties of  $[\text{Mn}(\text{im})(\text{CO})_3(\text{phen})]^+$  with those of the Re(I) analogue  $[\text{Re}(\text{im})(\text{CO})_3(\text{phen})]^+$  for which the steady-state and time-dependent spectroscopies, the ultrafast photophysics and the luminescent properties are well

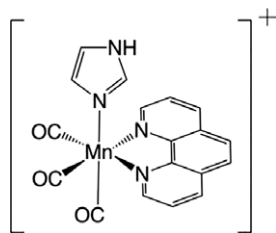
[a] M. Fumanal, E. Gindensperger, C. Daniel  
Laboratoire de Chimie Quantique, Institut de Chimie Strasbourg, UMR7177  
CNRS/Université de Strasbourg, 1 Rue Blaise Pascal, BP296/R8, Strasbourg  
F-67008, France  
E-mail: c.daniel@unistra.fr

[b] H. Yu, S. Maeda  
Department of Chemistry, Faculty of Science, Hokkaido University, Sapporo,  
Hokkaido, 060-0810, Japan  
E-mail: smaeda@eis.hokudai.ac.jp

[c] H. Yu, S. Maeda  
CREST, Japan Science and Technology Agency, Tokyo 102-8666, Japan

Contract grant sponsor: This work has been supported by Labex CSC (ANR-10-LABX-0026\_CSC) and French/Austrian ANR-15-CE29-0027-01 DeNeTheor. Contract grant sponsor: YH was supported by JST, PRESTO with grant number JPMJPR16N8. SM was supported by JST, CREST with grant number JPMJCR14L5.

© 2018 Wiley Periodicals, Inc.



Scheme 1. Structure of  $[\text{Mn}(\text{im})(\text{CO})_3(\text{phen})]^+$ .

documented, both experimentally and theoretically; (2) to explore the excited-state reactivity in first-row transition metal  $\alpha$ -diimine complexes, in particular to determine the dominant coordinates underlying the reactive decay. For this purpose, critical geometries (minima, transition states [TSs], and minimum energy conical intersection [MECI]) of multidimensional potential energy surfaces (PESs) are determined by means of gradient projection (GP)/single-component artificial force induced reaction (SC-AFIR) approach. A methodological by-product of this study is the validation of density functional theory (DFT) and time-dependent DFT (TD-DFT) electronic structure data within the context of both automatic PES investigations and subsequent quantum dynamics. Less dramatic for third-row transition metal complexes, this aspect is very important for first-row transition metal complexes due to significant electronic correlation effects. In this line, comparative complete-active-space self-consistent-field (CASSCF)/multistate CAS second-order perturbation theory (MS-CASPT2) results including spin-orbit coupling (SOC) and solvent effects are presented.

## Methods

### Electronic structure

Electronic structure calculations of  $[\text{Mn}(\text{im})(\text{CO})_3(\text{phen})]^+$  have been performed under  $C_s$  symmetry by means of DFT<sup>[23–25]</sup> including water solvent corrections based on a conductor-like screening model (COSMO).<sup>[26–28]</sup>

The calculations were performed using the B3LYP functional<sup>[29]</sup> and all electron triple- $\xi$  basis set.<sup>[30]</sup> The scalar relativistic effects were taken into account within the zeroth-order regular approximation.<sup>[31]</sup> The vertical transition energies were computed within TD-DFT<sup>[32,33]</sup> at the same level described above under the Tamm–Dancoff approximation (TDA).<sup>[34]</sup> The nonequilibrium solvation within the linear-response TD-DFT with a high-frequency dielectric constant of 1.77 for water is used. The SOC effects were introduced according to a simplified relativistic perturbative TD-DFT formalism.<sup>[35,36]</sup>

The electronic structure of the ground and excited states of the symmetric  $C_s$  conformer of  $[\text{Mn}(\text{im})(\text{CO})_3(\text{phen})]^+$  in its DFT/B3LYP minimum  $S_0$  geometry has also been determined at the state-average (SA)-CASSCF/MS-CASPT2 level of theory.<sup>[37–39]</sup> The atomic natural orbital relativistic consistent correlated ANO-RCC basis sets have been used considering the following contraction scheme: 21s15p10d6f4g2h/6s5p3d2f1g for Mn, 14s9p4d3f2g/4s3p2d1f for second-row atoms and 8s4p3d1f/2s1p for H.<sup>[40–42]</sup> A total of 14 electrons (eight  $\pi_{\text{phen}}$  and six  $3d_{\text{Mn}}$ ) are correlated into 14 active orbitals, including the seven doubly occupied described above,

two vacant  $3d_{\text{Mn}}$ , three pure  $\pi_{\text{phen}}^*$ , and two  $d\pi^*$  orbitals (14e14a). The lowest singlet and triplet excited states have been computed by means of SA-CASSCF (SA-RASSCF) calculations over 12 roots ( $^1A'$ ) and 11 roots ( $^1,^3A''$  and  $^3A'$ ). Solvent effects have been also evaluated in the case of a reduced 12e12a active space similar to the previous one but without one  $\pi/\pi^*$  set of  $a''$  orbitals and using the PCM model<sup>[43,44]</sup> considering the nonequilibrium solvation for the excited states. All CASPT2 calculations performed include all electrons except the deep-core (1s of C, N, and O, and 1s, 2s, 2p of Mn). The standard IPEA Hamiltonian<sup>[45]</sup> and the Cholesky decomposition<sup>[46]</sup> of two electron integrals has been used in all calculations, as well as an imaginary shift correction of 0.25 hartree to the external part of the zeroth-order Hamiltonian to avoid intruder-state problems.<sup>[47]</sup> Finally, the SOC effects have been evaluated using the restricted-active-space state-interaction spin-orbit method.<sup>[48]</sup>

The simulated absorption spectra have been obtained by means of a spectral line fitting using Gaussian functions of the TD-DFT transition energies and intensities. The excited-state character has been analyzed with TheoDORE<sup>[49,50]</sup> by means of electron-hole fragment decomposition as follows: F1 =  $\text{M}(\text{CO})_3$  ( $M = \text{Mn, Re}$ ); F2 = phen and F3 = im).

Density functional theory and TD-DFT calculations were performed with the ADF2013 code<sup>[51]</sup> and the CASSCF/MS-CASPT2 calculations with Molcas 8.2.<sup>[52]</sup>

To obtain an overview of the primary events taking place on the  $S_2$  PES that corresponds to the absorbing state, MECI structures and paths passing them were explored using the AFIR method.<sup>[53,54]</sup> MECIs between the first- and second-excited singlet states ( $S_1/S_2$ -MECIs) were searched by the single-component AFIR (SC-AFIR) algorithm combined with the GP type optimizer.<sup>[55]</sup> In the search, the structural deformation around the Mn center is explored by setting the target atoms in the SC-AFIR algorithm to seven atoms, that is, Mn, three carbon atoms in carbonyl, and three nitrogen atoms connected to the Mn atom. This search was done at the TD-DFT level under the TDA, with B3LYP functional including G3 type empirical dispersion corrections and water solvent corrections based on a conductor-like PCM model. In the initial automated search, LANL2DZ basis sets were adopted. All obtained MECIs were then reoptimized with cc-pVDZ basis sets. Connections of these MECIs on the  $S_1$  and  $S_2$  surfaces were studied by meta-intrinsic reaction coordinate (meta-IRC) calculations starting from these MECIs on each of the two surfaces, where meta-IRC corresponds to mass-weighted steepest descent path computed from nonstationary point.<sup>[56]</sup> TS structures for paths leading to these MECIs on  $S_2$  as well as those leading to dissociation channels on  $S_1$  were searched using the double-sphere AFIR (DS-AFIR) algorithm.<sup>[57]</sup> In these calculations, geometrical displacements were made by the GRRM program<sup>[58]</sup> using gradients computed by the Gaussian 16 program.<sup>[59]</sup>

## Results

### Electronic and structural properties of $[\text{Mn}(\text{im})(\text{CO})_3(\text{phen})]^+$ versus $[\text{Re}(\text{im})(\text{CO})_3(\text{phen})]^+$

The optimized geometry of  $[\text{Re}(\text{im})(\text{CO})_3(\text{phen})]^+$  in the  $S_0$  electronic ground state for its  $C_s$  conformer is presented in previous

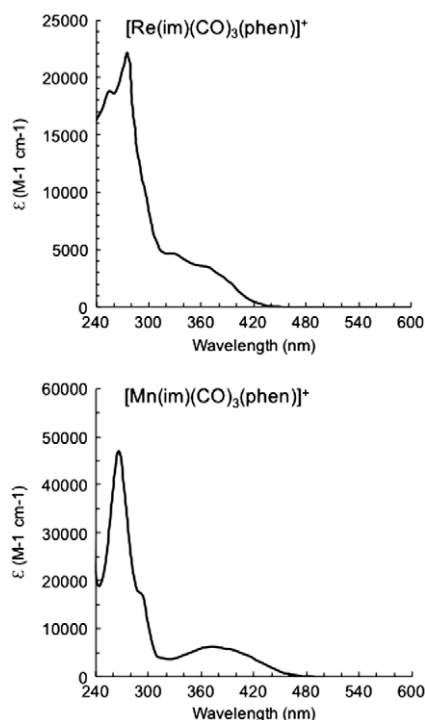


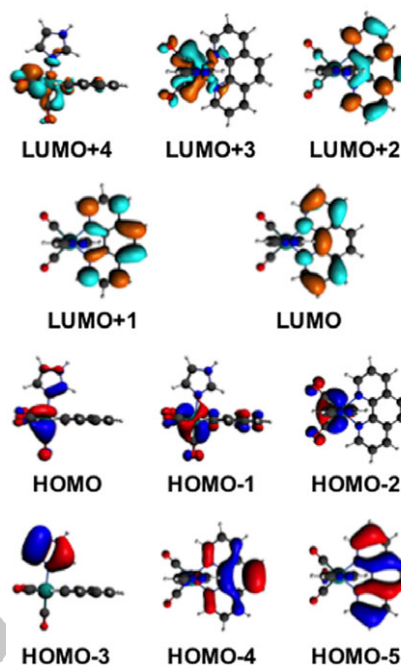
**Figure 1.** Experimental absorption spectra of  $[\text{Re}(\text{im})(\text{CO})_3(\text{phen})]^+$  in water and  $[\text{Mn}(\text{im})(\text{CO})_3(\text{phen})]^+$  in  $\text{CH}_2\text{Cl}_2$  adapted from Refs. <sup>[60]</sup> and <sup>[22]</sup>, respectively.

work.<sup>[12,13]</sup> When substituting the metal ion with Mn, the minimum energy structure of the  $S_0$  ground state of  $[\text{Mn}(\text{im})(\text{CO})_3(\text{phen})]^+$  is not significantly modified but only small deviations in the bond distances and angles are obtained. The important bond lengths and angles are reported for both compounds in Table 1 for comparison. It can be seen an important reduction of the metal–ligand distances of the DFT optimized structures in the case of the Mn complex in agreement with the X-ray experimental data reported, also collected in Table 1. The distances and angles concerning the carbonyl, phen, and imidazole ligands are not affected by the metal substitution, but only the ones of the metal–ligands coordination sphere due to the different size of the first-row and third-row metals.

The frontier ground state Kohn–Sham orbitals of  $[\text{Mn}(\text{im})(\text{CO})_3(\text{phen})]^+$  shown in Scheme 2 are equivalent to the ones of  $[\text{Re}(\text{im})(\text{CO})_3(\text{phen})]^+$  discussed in previous work.<sup>[12,13]</sup> No significant differences are observed in the shape and energy of the

**Table 1.** DFT optimized and X-ray important bond lengths (in Å) and bond angles (in °) of  $[\text{Re}(\text{im})(\text{CO})_3(\text{phen})]^+$  and  $[\text{Mn}(\text{im})(\text{CO})_3(\text{phen})]^+$  in water in the  $S_0$  electronic ground state.

	$M = \text{Re}$		$M = \text{Mn}$	
	X-ray <sup>[60]</sup>	$S_0$	X-ray <sup>[22]</sup>	$S_0$
M–N <sub>im</sub>	2.185	2.215	2.073	2.118
M–N <sub>phen</sub>	2.167/2.182	2.204	2.061/2.066	2.096
M–C <sub>ax</sub>	1.915	1.931	1.807/1.806	1.822
M–C <sub>eq</sub>	1.907/1.953	1.927	1.803	1.819
(C–C) <sub>phen</sub>	–	1.427	–	1.426
N <sub>phen</sub> –Re–N <sub>phen</sub>	75.8	75.0	79.4	78.6
C <sub>eq</sub> –Re–C <sub>eq</sub>	–	89.7	88.3	90.7
N <sub>im</sub> –Re–C <sub>ax</sub>	178.5	175.8	176.5	177.5
N <sub>phen</sub> –Re–N <sub>im</sub>	83.6/86.7	84.2	88.5	87.2



**Scheme 2.** Frontier ground state Kohn–Sham orbitals of  $[\text{Mn}(\text{im})(\text{CO})_3(\text{phen})]^+$ .

lowest empty and highest occupied molecular orbitals of the Mn complex with respect to the Re. On one side, the three highest HOMO correspond to the three d-like Mn–CO orbitals, the HOMO – 3 to a  $\pi^*$  localized in the im ligand, and the HOMO – 4 and HOMO – 5 to  $\pi^*$  localized in the phen. On the other side, the three lowest LUMO are  $\pi^*$  phen orbitals, and the LUMO + 3 and LUMO + 4 correspond to d-like Mn–CO unoccupied orbitals. Similar frontier MOs in both metal complexes would indicate that no significant differences are expected in the lowest energy spectra and excited-state manifold of both complexes. However, the orbital picture does not always correspond to a realistic picture of the excited-state properties and only explicit excited-state calculations provide a proper comparison. This is discussed in the next section.

### Absorption spectroscopy of $[\text{Mn}(\text{im})(\text{CO})_3(\text{phen})]^+$ versus $[\text{Re}(\text{im})(\text{CO})_3(\text{phen})]^+$ and SOC

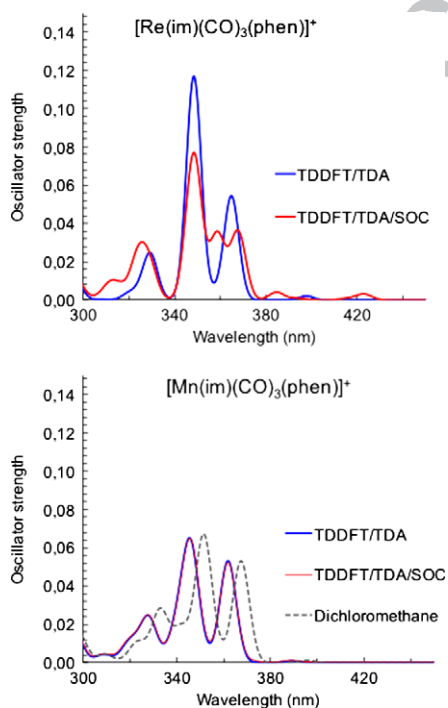
The experimental absorption spectra of  $[\text{Re}(\text{im})(\text{CO})_3(\text{phen})]^+$  in water,<sup>[60]</sup> and the one of  $[\text{Mn}(\text{im})(\text{CO})_3(\text{phen})]^+$  complex in dichloromethane<sup>[22]</sup> are reproduced in Figure 1. Very similar features are seen in both cases: they start at 440 and 480 nm, respectively, and display a broad low-energy band up to 320 nm assigned to the lowest MLCT transitions. The shift to the red of this MLCT band in the case Mn is ascribed to the lower polarity of the dichloromethane solvent with respect to water. The bright peaks between 240 and 300 nm are attributed to IL transitions.

The TD-DFT/TDA calculated absorption spectra of  $[\text{Re}(\text{im})(\text{CO})_3(\text{phen})]^+$  in water has been previously discussed.<sup>[12,13,18]</sup> The absorption spectra of  $[\text{Mn}(\text{im})(\text{CO})_3(\text{phen})]^+$  computed under the same conditions is presented here in Figure 2 together with the one of  $[\text{Re}(\text{im})(\text{CO})_3(\text{phen})]^+$  for comparison.



1 Moreover, the spectrum of  $[\text{Mn}(\text{im})(\text{CO})_3(\text{phen})]^+$  in dichloro-  
 2 methane is also shown to assess the role of the solvent polarity  
 3 in the position of the lowest peaks (dashed line in Fig. 2). Note  
 4 that a proper comparison with the experimental spectrum can  
 5 only be achieved when several conformers of the complex are  
 6 considered.<sup>[12,18]</sup> As expected from the molecular orbital picture  
 7 (see previous section), both complexes present very similar fea-  
 8 tures. The peaks at 365, 349, and 329 nm that characterize the  
 9 SO-free spectrum of  $[\text{Re}(\text{im})(\text{CO})_3(\text{phen})]^+$  in water appear at  
 10 362, 346, and 328 nm for  $[\text{Mn}(\text{im})(\text{CO})_3(\text{phen})]^+$  in the same  
 11 conditions. Notably, these peaks move to 368, 352, and 333 nm  
 12 when computed in dichloromethane. The full TD-DFT/TDA data  
 13 including the vertical transition energies of the low-lying singlet  
 14 and triplets, wavelengths of absorption, oscillator strengths,  
 15 and most important one-electron excitations of  $[\text{Mn}(\text{im})$   
 16  $(\text{CO})_3(\text{phen})]^+$  in water are collected in Supporting Information  
 17 Table S1, together with the data of  $[\text{Re}(\text{im})(\text{CO})_3(\text{phen})]^+$  for  
 18 comparison.<sup>[12,13]</sup> A careful analysis of the excited states com-  
 19 position indicates that the same one-electron excitations char-  
 20 acterize the absorbing peaks in both complexes. In particular,  
 21 the lowest band corresponds mainly to the HOMO - 1  $\rightarrow$  LUMO  
 22 transition and the second one to HOMO  $\rightarrow$  LUMO + 1.

23 The lowest singlet and triplet excited states up to the lowest  
 24 absorbing peak in the visible are collected in Table 2 for  $[\text{Re}(\text{im})$   
 25  $(\text{CO})_3(\text{phen})]^+$  and  $[\text{Mn}(\text{im})(\text{CO})_3(\text{phen})]^+$  in water. In both cases,  
 26 the lowest strong absorbing state corresponds to  $S_2$  of A' sym-  
 27 metry and is ascribed to the MLCT transition. Remarkably, the  
 28 number of triplet states below  $S_2$  is much larger for the Mn  
 29 complex than for the Re complex (Fig. 3). In the case of Re,  
 30 there are two low-lying triplet states of MLCT character ( $T_1$  and  $T_2$ ),



31  
32  
33  
34  
35  
36  
37  
38  
39  
40  
41  
42  
43  
44  
45  
46  
47  
48  
49  
50  
51  
52  
53  
54  
55  
56  
57  
**Figure 2.** TD-DFT/TDA absorption spectrum of  $[\text{Re}(\text{im})(\text{CO})_3(\text{phen})]^+$  (left) and  $[\text{Mn}(\text{im})(\text{CO})_3(\text{phen})]^+$  computed in water without and with the SOC effects. The calculated spectrum of  $[\text{Mn}(\text{im})(\text{CO})_3(\text{phen})]^+$  in  $\text{CH}_2\text{Cl}_2$  solvent is also shown in dotted-line.

**Table 2.** TD-DFT/TDA transition energies (in eV), wavelengths of absorption (in nm), and oscillator strengths  $f$  associated to the low-lying "spin-free" singlet and triplet excited states of  $[\text{Re}(\text{im})(\text{CO})_3(\text{phen})]^+$  and  $[\text{Mn}(\text{im})(\text{CO})_3(\text{phen})]^+$  in water.

State	Character	Transition energy	Wave length	$f$
$M = \text{Re}$				
$T_1A''$	$\text{ML}_{\text{phen}}\text{CT}$	2.98	416	
$T_2A'$	$\text{ML}_{\text{phen}}\text{CT}$	3.07	403	
$T_3A''$	$\text{ML}_{\text{phen}}\text{CT}/\text{IL}_{\text{phen}}$	3.24	382	
$S_1A''$	$\text{ML}_{\text{phen}}\text{CT}$	3.12	398	0.002
$S_2A'$	$\text{ML}_{\text{phen}}\text{CT}$	3.40	365	0.054
$T_4A'$	$\text{ML}_{\text{phen}}\text{CT}$	3.42	363	
$M = \text{Mn}$				
$T_1A'$	MC	2.92	425	
$T_2A''$	$\text{ML}_{\text{phen}}\text{CT}$ (MC)	2.95	420	
$T_3A'$	$\text{ML}_{\text{phen}}\text{CT}$ (MC)	3.09	401	
$T_4A''$	MC	3.10	400	
$T_5A''$	$\text{ML}_{\text{phen}}\text{CT}$ ( $\text{IL}_{\text{phen}}/\text{MC}$ )	3.17	391	
$S_1A''$	$\text{ML}_{\text{phen}}\text{CT}$	3.19	389	0.001
$T_6A''$	MC	3.22	385	
$T_7A'$	$\text{MC}/\text{ML}_{\text{phen}}\text{CT}$	3.23	384	
$T_8A''$	$\text{ML}_{\text{phen}}\text{CT}$ (MC)	3.32	373	
$T_9A'$	$\text{MC}/\text{ML}_{\text{phen}}\text{CT}$	3.34	371	
$S_2A'$	$\text{ML}_{\text{phen}}\text{CT}$	3.43	362	0.053
$T_{10}A'$	$\text{ML}_{\text{phen}}\text{CT}$ ( $\text{IL}_{\text{phen}}$ )	3.48	356	

and one partial  $\text{IL}_{\text{phen}}$  ( $T_3$ ) excited state below  $S_2$ , while  $T_4$  lies slightly above.<sup>[12,13]</sup> These MLCT (and partial IL) excited states are also found in the Mn complex as  $T_2$ ,  $T_3$ ,  $T_5$ , and  $T_{10}$ , respectively. However, they are importantly mixed with MC one-electron contributions. In addition, several pure MC ( $T_1$ ,  $T_4$ , and  $T_6$ ) and partial MC ( $T_7$ ,  $T_8$ , and  $T_9$ ) states appear in the case of Mn complex, largely increasing the number of excited states at low energies (from 4 to 10). This is in contrast to the similar orbital picture that both complexes show in their ground state (see previous section) and indicates that only an excited-state analysis (here by means of TD-DFT) can provide a realistic scenario of the low-lying excited-state manifold. Given that these extra excited states in the case of the Mn complex correspond to dark states, they do not contribute to the absorption and both complexes show very similar absorbing properties (Fig. 2).

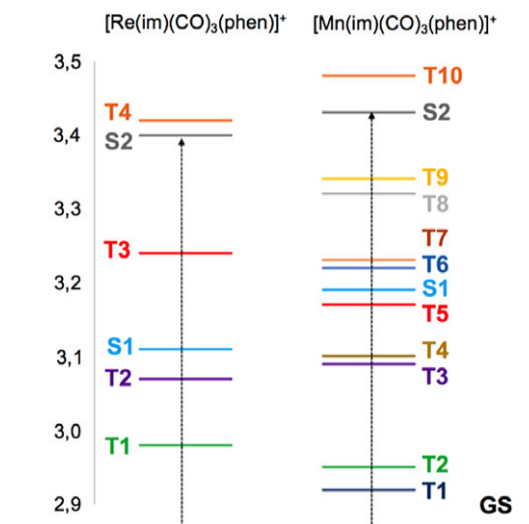


**Figure 3.** TD-DFT/TDA transition energies (in eV) of the low-lying spin-orbit free excited state manifold of  $[\text{Re}(\text{im})(\text{CO})_3(\text{phen})]^+$  and  $[\text{Mn}(\text{im})(\text{CO})_3(\text{phen})]^+$  in COSMO water.

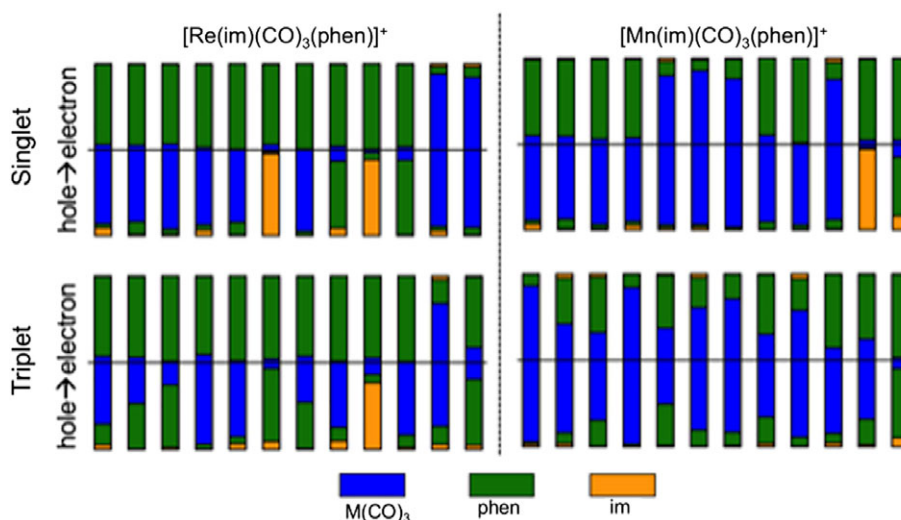


**Figure 4.** Excited state character of the lowest singlet and triplet states of  $[\text{Re}(\text{im})(\text{CO})_3(\text{phen})]^+$  and  $[\text{Mn}(\text{im})(\text{CO})_3(\text{phen})]^+$ .

Nevertheless, very different photophysical behaviors are expected after photo absorption in the visible as a consequence of the potential participation of these new low-lying MC triplets in the excited-state decay of  $S_2$ .

The excited-state character of the 12 lowest singlet and triplet states of  $[\text{Re}(\text{im})(\text{CO})_3(\text{phen})]^+$  and  $[\text{Mn}(\text{im})(\text{CO})_3(\text{phen})]^+$  is represented in Figure 4 by means of electron-hole fragment decomposition diagrams obtained from TheoDORE analysis.<sup>[49,50]</sup> Each excited state is represented as a vertical bar in which the color below and above the midline indicates the fragments that contribute into the hole and electron densities, respectively. That is, the MC and IL states are shown as blue-blue and green-green electron-hole bars, respectively, while the charge transfer MLCT and LLCT (ligand-to-ligand-charge-transfer) states are shown as green-blue and green-yellow bars in which the electron is promoted from the metal and the im ligand, respectively, to the phen ligand. It can be seen that in both complexes the lowest singlets correspond to pure MLCT states, however in the case of  $[\text{Mn}(\text{im})(\text{CO})_3(\text{phen})]^+$  the MC singlet states ( $S_5$ – $S_7$ ) appear below the lowest LLCT ( $S_{11}$ ) and IL ( $S_{12}$ ) contributions, in contrast to  $[\text{Re}(\text{im})(\text{CO})_3(\text{phen})]^+$  for which the lowest MC corresponds to  $S_{11}$ . The lowest triplet manifold of  $[\text{Mn}(\text{im})(\text{CO})_3(\text{phen})]^+$  is characterized by MC and MLCT states, while only MLCT, IL, and LLCT contributions appear in the case of  $[\text{Re}(\text{im})(\text{CO})_3(\text{phen})]^+$  until  $T_{11}$ .

The six “spin-orbit free” low-lying singlet and triplet excited states of  $[\text{Re}(\text{im})(\text{CO})_3(\text{phen})]^+$  give rise to 14 largely mixed “spin-orbit” states when SOC is considered.<sup>[12,13,17]</sup> Large SOC terms and mixings characterize the Re complex as expected for a heavy metal atom complex and the general trends when including SOC are observed in the SO simulated spectrum, that is a shift to the red of the lowest bands and a lowering of the intensities (Fig. 2). In contrast, the SO simulated spectrum of Mn does not show any difference with the “SO-free” spectrum (see Fig. 2) and both are almost perfectly superimposed. The SO excited states arising from the two low-lying singlets and nine triplets of  $[\text{Mn}(\text{im})(\text{CO})_3(\text{phen})]^+$ , and the SOC terms between them, are collected in Supporting Information Tables S2 and S3, respectively. Small SO mixings characterize the Mn complex, as well as SOC terms significantly smaller in  $[\text{Mn}(\text{im})(\text{CO})_3(\text{phen})]^+$  (up to ca. 100  $\text{cm}^{-1}$ ) than the ones previously reported for  $[\text{Re}(\text{im})(\text{CO})_3(\text{phen})]^+$  (up to ca. 600  $\text{cm}^{-1}$ ). These results are in agreement with a small SO contribution for a first-row coordination complex with respect to its third-row analogues, and would tentatively indicate that intersystem-crossing is disfavored with respect to internal-conversion in the case of Mn.

The above description of excited states in  $[\text{Mn}(\text{im})(\text{CO})_3(\text{phen})]^+$  based on TD-DFT results is discussed by comparison with MS-CASPT2 data in the following section.

**Table 3.** CASSCF/MS-CASPT2 and TD-DFT transition energies (in eV) and character of the low-lying singlet excited states of  $[\text{Mn}(\text{im})(\text{CO})_3(\text{phen})]^+$ .

CASSCF(14e1a)/MS-CASPT2 without solvent correction			CASSCF(12e12a)/ MS-CASPT2 with solvent correction <sup>[a]</sup>		TD-DFT(B3LYP)/COSMO		
State	Character	Transition energy	Character	Transition energy	State	Character	Transition energy
$a^1A''$	MC/MLCT	3.59	MC/MLCT	3.40	$a^1A''$	MLCT	3.19
$b^1A''$	MLCT/MC	3.62	MLCT/MC	3.42	$b^1A'$	MLCT	3.43
$b^1A'$	MLCT	3.73	MLCT	3.70 (3.71)	$c^1A'$	MLCT	3.52
$c^1A'$	MLCT	3.80	MLCT	3.78 (3.79)	$b^1A''$	MC	3.56
$d^1A'$	<b>MLCT</b>	<b>3.89</b>	<b>MC</b>	<b>3.82 (3.84)</b>	$d^1A'$	MLCT	3.59
$c^1A''$	<b>MLCT</b>	<b>3.96</b>	<b>MC</b>	<b>3.91</b>	$e^1A'$	MC	3.64
$d^1A''$	MLCT	4.06	MLCT	4.08	$c^1A''$	MC	3.69
$e^1A'$	<b>MC</b>	<b>4.10</b>	<b>MLCT</b>	<b>3.94 (3.97)</b>	$d^1A''$	MLCT	3.78
$e^1A''$	<b>MC</b>	<b>4.11</b>	<b>MLCT</b>	<b>4.15</b>	$e^1A''$	MLCT	3.87

[a] The transition energies in parenthesis correspond to the calculated values without solvent correction.

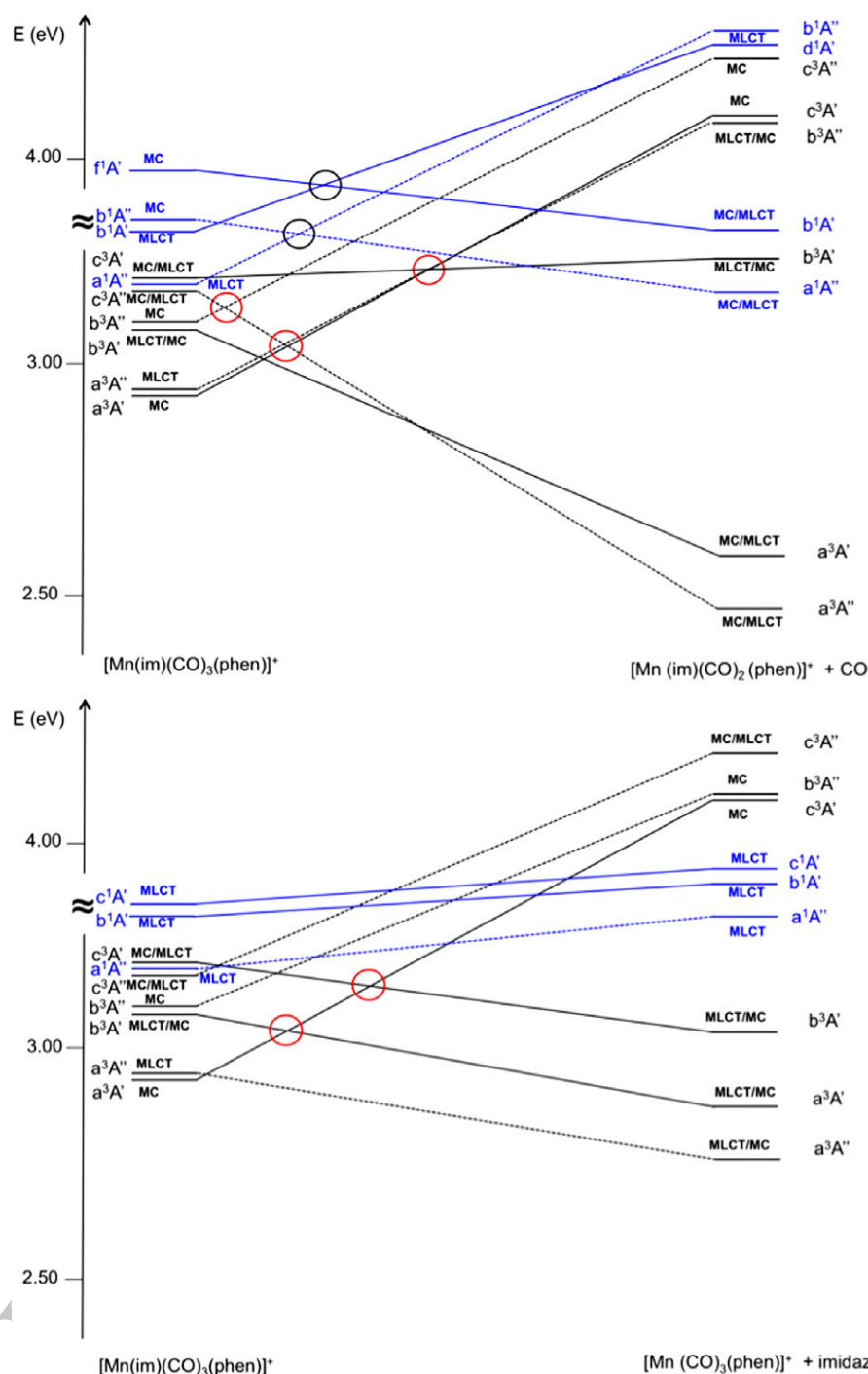


**Figure 5.** State diagrams correlating the low-lying singlet and triplet states of  $[\text{Mn}(\text{im})(\text{CO})_3(\text{phen})]^+$  to the corresponding states of the  $[\text{Mn}(\text{im})(\text{CO})_2(\text{phen})]^+ + \text{CO}_{\text{ax}}$  and  $[\text{Mn}(\text{CO})_3(\text{phen})]^+ + \text{imidazole}$  primary products associated to the  $\text{CO}_{\text{ax}}$  loss (top) and the Mn–imidazole bond breaking (bottom).

### Low-lying excited states analysis at FC by means of CASSCF/MS-CASPT2

Whereas the TD-DFT method is appropriate for describing lowest electronic excited states in a number of second- and third-row transition metal complexes<sup>[11,61,62]</sup> its use for first-row transition metal complexes is more questionable.<sup>[63–65]</sup> Indeed, describing on the same footing MLCT and MC excited states is a real challenge for computational chemistry. The TD-DFT/B3LYP/COSMO and MS-CASPT2/CASSCF transition energies of

the lowest singlet and triplet excited states of  $[\text{Mn}(\text{im})(\text{CO})_3(\text{phen})]^+$  are compared in Table 3 and Supporting Information Table S4, respectively. The PCM solvent correction has been applied only to the CASSCF limited to 12 active orbitals because of computational limitations. As illustrated by the data reported in Table 3 for the low-lying  $^1A'$  excited states the solvent correction has negligible effect on the computed MS-CASPT2 transition energies. Both CASSCF/MS-CASPT2 calculations, namely, 12e12a limited to 6/5 roots and 14e14a expanded to 12/11 roots give the same sequence of low-lying

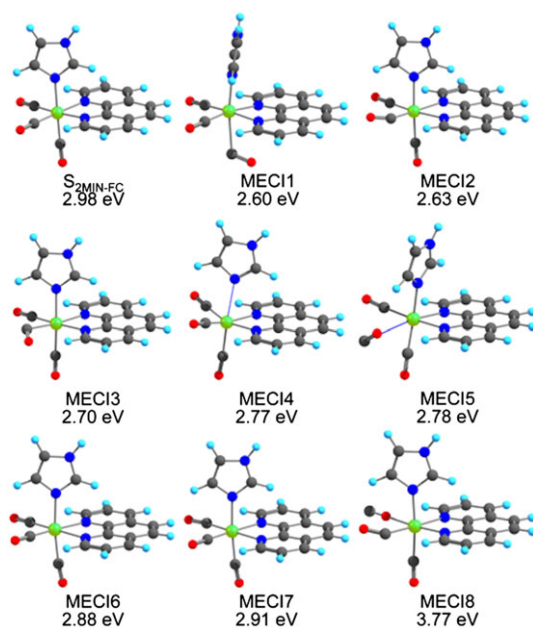


**Figure 6.** Geometries of  $S_2$  local minimum nearest to the FC geometry ( $S_{2\text{MIN-FC}}$ ) and all obtained  $S_1/S_2$ -MECIs ( $S_1/S_2$ -MECI1–8). Energies are relative to the  $S_0$  energy at the FC geometry.

singlet states with similar transition energies, blue-shifted with respect to the experimental absorption band and to the TD-DFT transition energies. When giving less electronic flexibility by limiting the CASSCF active space and decreasing the number of requested roots the MC states are stabilized by exchanging the  $d^1A'$  and  $c^1A''$  states with the  $e^1A'$  and  $e^1A''$  excited states (Table 3, in bold). However, both calculations exhibit the six MLCT and three MC states that characterize the investigated domain of energy. Importantly and in contrast with TD-DFT the two lowest singlet states of  $A''$  symmetry,  $a^1A''$  and  $b^1A''$ , are characterized by a mixed MC/MLCT character and nearly degenerate. TD-DFT gives two well separate states by 0.37 eV  $a^1A''$  (MLCT) and  $b^1A''$  (MC). The three lowest pure MLCT states,  $b^1A'$ ,  $c^1A'$ , and  $d^1A'$  are well reproduced at the TD-DFT level of theory that shift their energies by about 0.3 eV providing a better agreement with experimental absorption band. Similarly, the upper MLCT and MC states ( $c^1A''$ ,  $d^1A''$ ,  $e^1A''$ , and  $e^1A'$ ) obtained at the CASSCF (14e14a)/MS-CASPT2 level are well reproduced by TD-DFT.

The comparison performed on the low-lying triplet states (Supporting Information Table S4) follows the same trends. The qualitative agreement between TD-DFT and MS-CASPT2 results should not obscure two limits: (1) the fortuitous agreement between TD-DFT results and experimental data; (2) the room for improvement of the CASSCF/MS-CASPT2 results. Indeed, on one hand TD-DFT results are obtained with a specific functional combined with linear-response theory and solvent correction based on a cavity model. It is probable that cancellations of error lead to reasonable transition energies. On the other hand, modifying the quality of the CASSCF wavefunction in size or in terms of active orbitals (more  $\pi^*$  orbitals for instance) and requested roots, performing wavefunction/perturbation on a

structure optimized at the MS-CASPT2 level could change the relative ordering of the MLCT and MC states.

### State correlation diagrams for Mn–CO<sub>ax</sub> and Mn–imidazole elongation in $[\text{Mn}(\text{im})(\text{CO})_3(\text{phen})]^+$

To qualitatively investigate the potential reactivity of  $[\text{Mn}(\text{im})(\text{CO})_3(\text{phen})]^+$  in water, we built state correlation diagrams for the axial CO departure, as well as for the Mn–imidazole bond breaking. The low-lying excited states of  $[\text{Mn}(\text{im})(\text{CO})_3(\text{phen})]^+$  described above were correlated to the corresponding ones of the  $[\text{Mn}(\text{im})(\text{CO})_2(\text{phen})]^+ + \text{CO}_{\text{ax}}$  and  $[\text{Mn}(\text{CO})_3(\text{phen})]^+ + \text{imidazole}$  primary products on the basis of TD-DFT/TDA transition energies computed at fixed distances of the leaving ligand (8 Å), symmetry considerations and state character. No geometrical relaxation is considered and the  $C_s$  symmetry is conserved at this qualitative level, the goal of which is to identify the potentially reactive excited states for both channels. The resulting state correlation diagrams are shown in Figure 5 and the excited-state difference densities are collected in Supporting Information Figures S1 and S2.

Under the  $C_s$  symmetry constraint, three low-lying triplet states, namely,  $a^3A''$  ( $T_2$ ),  $b^3A'$  ( $T_3$ ), and  $c^3A'$  ( $T_6$ ) are weakly dissociative along the Mn–imidazole bond elongation, whereas two low-lying triplet states, namely,  $b^3A'$  ( $T_3$ ) and  $c^3A''$  ( $T_5$ ) are strongly dissociative along the Mn–CO<sub>ax</sub> bond elongation. This generates potentially conical intersections within a multidimensional picture as exemplified by red circles in Figure 5 along the axial CO and im dissociation pathways. Interestingly, the low-lying dissociative triplet states keep major MLCT character in the primary products corresponding to the imidazole departure whereas they gain major MC character in  $[\text{Mn}(\text{im})(\text{CO})_2(\text{phen})]^+ + \text{CO}_{\text{ax}}$  leading to an important stabilization. Two singlet states of MC character are weakly dissociative along the Mn–CO<sub>ax</sub> bond dissociation path, namely, the  $b^1A''$  ( $S_4$ ) and  $f^1A'$  ( $S_9$ ) and cross the lowest bound MLCT states  $a^1A'$  ( $S_1$ ) and  $b^1A'$  ( $S_2$ ) generating mixed MC/MLCT singlet states at dissociation. In a one-dimensional view and on the basis of this qualitative analysis we expect that the two lowest  $S_1$  and  $S_2$  singlet states are weakly dissociative for the CO loss with energy barriers generated nearby the FC region by avoided crossing with the upper MC states (exemplified by black circles in Fig. 5).

This suggests that a further analysis has to include other important degrees of freedom, eventually breaking the symmetry that will assist the CO<sub>ax</sub> dissociation. Alternatively, an effective spin-vibronic mechanism similar to the one revealed for  $[\text{Re}(\text{im})(\text{CO})_3(\text{phen})]^{+[\text{17}]}$  could as well populate efficiently the low-lying dissociative triplet states.

To investigate more in details the singlet excited-state PESs of  $[\text{Mn}(\text{im})(\text{CO})_3(\text{phen})]^+$  we have performed a systematic search of critical geometries.

### $[\text{Mn}(\text{im})(\text{CO})_3(\text{phen})]^+$ critical geometries and energy profiles

Although different basis sets (cc-pVDZ) and computational program (Gaussian 16) were used in the stationary point calculations, results at FC were qualitatively similar to those discussed



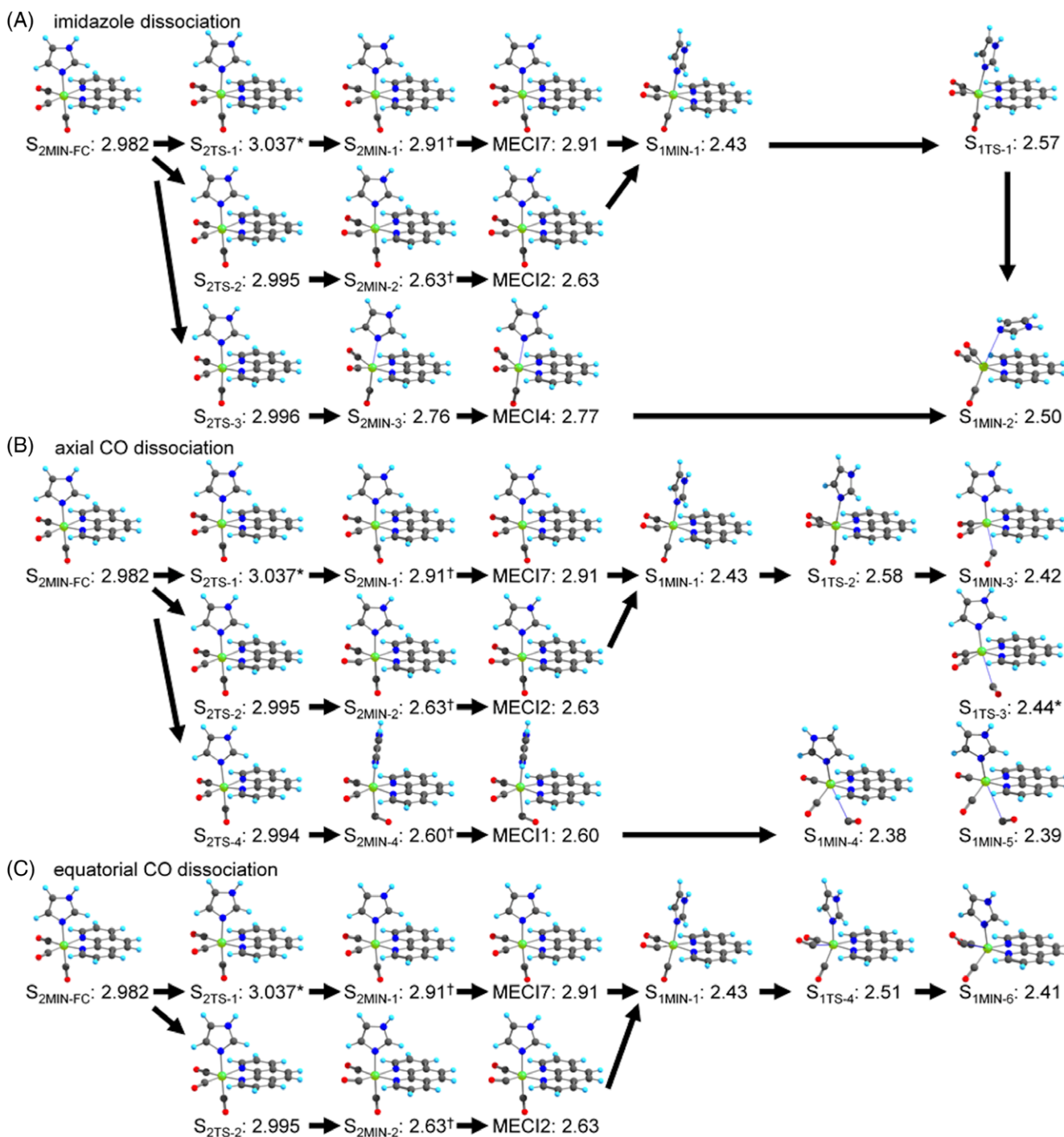


**Figure 7.** Pathways from  $S_{2MIN-FC}$  to dissociated structures on  $S_1$ : (a) for imidazole dissociation, (b) for axial CO dissociation, and (c) for equatorial CO dissociation. Energies are shown in eV relative to  $S_{0MIN}$ . Note that  $S_{2MIN-1}$ ,  $S_{2MIN-2}$ , and  $S_{2MIN-4}$  are located inside the corresponding CIs, that is, MECI7, MECI2, and MECI1, respectively; the geometries for  $S_{2MIN-1}$ ,  $S_{2MIN-2}$ , and  $S_{2MIN-4}$  are identical to MECI1, MECI2, and MECI1 geometries. These are indicated by “†.” Two TSs,  $S_{2TS-1}$  and  $S_{1TS-3}$ , did not converge because of very shallow PES around them.  $S_{2TS-1}$  and  $S_{1TS-3}$  indicated with “\*” correspond to the highest energy point along a relaxed interpolation path, and the relaxed interpolation paths are shown in Supporting Information Figure S3.

above. The bright state is  $S_2$  (0.003 for  $S_1$  and 0.079 for  $S_2$ ), and excitation energies to  $S_1$  and  $S_2$  at the FC geometry are 3.02 and 3.27 eV, respectively. These correspondences to the above results would justify the use of this computational level in the stationary point search.

Figure 6 lists all obtained  $S_1/S_2$ -MECIs near the FC geometry. There are four types with substantial importance: (1) imidazole

dissociation (MECI4), (2) axial CO bent type (MECI1), (3) equatorial CO bent type (MECI2 and MECI3), and (4) axial/equatorial CO bent type (MECI6 and MECI7). In the axial/equatorial CO bent type, both axial and equatorial CO are slightly bent. Between the two equatorial CO bent type MECIs, MECI2 is closer to  $S_{2MIN-FC}$  and more important than MECI3. In other words, the system must pass the MECI2 region before reaching

1 the MECI3 region; the DS-AFIR path between the FC region and  
2 the MECI3 region had two barriers and the MECI2 region lied  
3 between the two barriers. Also, an equatorial CO dissociation  
4 type (MECI5) is not important because the MECI region for the  
5 equatorial CO bent type must be passed before reaching it. The  
6 DS-AFIR path between the FC region and the MECI5 region had  
7 three barriers and an intermediate region including MECI3.  
8 Another minor one is MECI8 in which CO coordinates to Mn  
9 with oxygen atom in one of equatorial sites.

10 Minimum energy conical intersections of these four types  
11 may lead to decomposition of  $[\text{Mn}(\text{im})(\text{CO})_3(\text{phen})]^+$ . All possi-  
12 ble paths and the energies on the critical points along the  
13 paths are shown in Figure 7: (1) for imidazole dissociation,  
14 (2) for axial CO dissociation, and (3) for equatorial CO disso-  
15 ciation. The imidazole dissociation occurs through two paths. One  
16 is a direct path through MECI4. The meta-IRC calculation on  $S_1$   
17 surface from the geometry of MECI4 directly led the imidazole  
18 dissociation. Another takes place via  $S_{1\text{MIN}-1}$ , which is generated  
19 through either equatorial CO bent, or axial/equatorial CO bent  
20 type MECI. The axial CO dissociation also occurs either directly  
21 through MECI or indirectly via  $S_{1\text{MIN}-1}$ . Conversely, the equatorial  
22 CO dissociation occurs only indirectly from  $S_{1\text{MIN}-1}$ .

23 The two direct paths for the imidazole dissociation and the  
24 axial CO dissociation compete to each other, because their bar-  
25 riers, that is,  $S_{2\text{TS}-3}$  and  $S_{1\text{TS}-4}$ , are nearly identical. Moreover, the  
26 direct axial CO dissociation path is more preferable than the  
27 indirect paths.

28 Among the indirect paths via  $S_{1\text{MIN}-1}$ , the equatorial CO disso-  
29 ciation path through  $S_{1\text{TS}-4}$  (2.51 eV) is energetically most favor-  
30 able. The imidazole dissociation occurs in one-step through  
31  $S_{1\text{TS}-1}$  (2.57 eV). The axial CO dissociation from  $S_{1\text{MIN}-1}$  occurs in  
32 two-step via  $S_{1\text{TS}-2}$  and  $S_{1\text{TS}-3}$ , and  $S_{1\text{TS}-2}$  (2.58 eV) is its rate-  
33 determining step. Interestingly, all paths involve a rotation of  
34 the imidazole, which will likely slow down the speed of bond  
35 breaking.

36 All these channels highly compete to each other. Among  
37 them, the direct axial CO dissociation is energetically most pre-  
38 ferred. Therefore, from the energetic consideration, we con-  
39 clude that the axial CO dissociation is the most favorable  
40 channel. However,  $S_{2\text{TS}-2}$ ,  $S_{2\text{TS}-3}$ , and  $S_{2\text{TS}-4}$  leading to equatorial  
41 CO bent, imidazole dissociation and axial CO bent types,  
42 respectively, have almost same barriers. Also, all the dissociation  
43 channels from  $S_{1\text{MIN}-1}$  in  $S_1$  are energetically very close to each  
44 other. Their preference may change depending on computa-  
45 tional level adopted and/or dynamical effects. A further dynam-  
46 ics study on highly accurate PESs or an experimental study will  
47 be required to discuss the branching ratio accurately. Our study  
48 identified all these possibilities by the automated SC-AFIR  
49 search, and we hope that these results stimulate further com-  
50 putational and experimental studies.

51 A recent experimental study has reported the discovery of  
52 the first fluorescent manganese carbonyl-based PhotoCORM  
53  $[\text{Mn}(\text{Imdansyl})(\text{CO})_3(\text{phen})]$   $[\text{CF}_3\text{SO}_3]$   
54 (Imdansyl = dansylimidazole) very similar to the presently inves-  
55 tigated complex.<sup>[66]</sup> This corroborates our hypothesis of two  
56 concurrent channels in this class of Mn(II) complexes, namely,  
57 fluorescence and carbonyl dissociation.

## Conclusion


The electronic excited states properties and reactivity of  $[\text{Mn}(\text{imid-azole})(\text{CO})_3(\text{phen})]^+$  have been investigated by means of both DFT and wavefunction electronic structure calculations supplemented by a systematic exploration of the associated PESs. Whereas the electronic ground state properties of the complex are very similar to those of the Re(I) analogue, the sequence of low-lying excited states differ drastically. Indeed, the Mn(II) complex is characterized by a high density of singlet and triplet MC, MLCT, and IL states within 0.56 eV while the Re(I) complex exhibits a reduced number of MLCT states in the same energy domain. Both complexes absorb at about 400 and 360 nm and their absorption spectra present similar features. TD-DFT/B3LYP/COSMO transitions energies and state characters are validated by CASSCF/MS-CASPT2 calculations. On the basis of qualitative state correlation diagrams that connect the low-lying excited states of the parent molecule to those of the fragments  $[\text{Mn}(\text{imidazole})(\text{CO})_2(\text{phen})]^+ + \text{CO}_{\text{ax}}$  and  $[\text{M}(\text{CO})_3(\text{phen})]^+ + \text{Imidazole}$ , two dissociative channels are considered. The two lowest  $S_1$  and  $S_2$  singlet states are weakly dissociative for the CO loss with energy barriers generated nearby the FC region. A further analysis based on a systematic search of pathways from  $S_2$  minimum at FC to dissociated structures on  $S_1$  indicates that the direct axial CO loss is energetically most favorable. However, other channels leading to equatorial CO bent, imidazole dissociation or axial CO bent are competitive.

## Acknowledgments

This work has been supported by Labex CSC (ANR-10-LABX-0026\_CSC) and French/Austrian ANR-15-CE29-0027-01 DeNeTheor. The calculations have been performed at the High Performance Computer Centre (HPC), University of Strasbourg and on the nodes cluster of the Laboratoire de Chimie Quantique. YH was supported by JST, PRESTO with grant number JPMJPR16N8. SM was supported by JST, CREST with grant number JPMJCR14L5. A part of the results was computed at the computer center of Kyoto University.

**Keywords:** quantum chemistry · spin-orbit coupling · absorption spectroscopy · rhenium (I) complexes · density functional theory · wave function · CO release · Mn complexes

How to cite this article: M. Fumanal, H. Yu, E. Gindensperger, S. Maeda, C. Daniel. *J. Comput. Chem.* **2018**, 9999, 1–11. DOI: 10.1002/jcc.25535

 Additional Supporting Information may be found in the online version of this article.

- [1] R. D. Rimmer, A. E. Pierr, P. C. Ford, *Coord. Chem. Rev.* **2012**, 256, 1509.
- [2] J. S. Ward, J. M. Lynam, J. W. B. Moir, D. E. Sanin, A. P. Mountford, I. J. S. Fairlamb, *Dalton Trans.* **2012**, 41, 10514.
- [3] C. Long, In *Topics in Organometallics Chemistry*, Vol. 29; A. J. Lee, Ed., **2010**, p. 37.
- [4] D. Guillaumont, A. Vlček, Jr., C. Daniel, *J. Phys. Chem. A* **2001**, 105, 1107.
- [5] R. Farrel, P. Matousek, M. Towrie, A. W. Parker, D. C. Grills, M. W. George, A. Vlček, Jr., *Inorg. Chem.* **2002**, 17, 4318.

- [6] A. Vlček, Jr., *Coord. Chem. Rev.* **2002**, 230, 225.
- [7] S. Mc Mahon, S. Amirjalayer, W. J. Buma, Y. Halpin, C. Long, A. D. Rooney, S. Woutersen, M. T. Pryce, *Dalton Trans.* **2015**, 44, 15424.
- [8] A. El Nahhas, C. Consani, A. M. Blanco-Rodríguez, K. M. Lancaster, O. Braem, A. Cannizzo, M. Towrie, I. P. Clark, S. Zálaiš, M. Chergui, A. Vlček, Jr., *Inorg. Chem.* **2011**, 50, 2932.
- [9] A. Cannizzo, A. M. Blanco-Rodríguez, A. El Nahhas, J. Sebera, S. Zálaiš, A. Vlček, Jr., M. Chergui, *J. Am. Chem. Soc.* **2008**, 130, 8967.
- [10] A. El Nahhas, A. Cannizzo, F. van Mourik, A. M. Blanco-Rodríguez, S. Zálaiš, A. Vlček, Jr., M. Chergui, *J. Phys. Chem. A* **2010**, 114, 6361.
- [11] R. Heydova, E. Gindensperger, R. Romano, J. Sykora, A. Vlček, S. Zálaiš, C. Daniel, *J. Phys. Chem. A* **2012**, 116, 11319.
- [12] M. Fumanal, C. Daniel, *J. Comput. Chem.* **2016**, 37, 2454.
- [13] M. Fumanal, C. Daniel, *J. Phys. Chem. A* **2016**, 120, 6934.
- [14] C. Gourlaouen, J. Eng, M. Otsuka, E. Gindensperger, C. Daniel, *J. Chem. Theory Comput.* **2015**, 11, 99.
- [15] J. Eng, C. Gourlaouen, E. Gindensperger, C. Daniel, *Acc. Chem. Res.* **2015**, 48, 809.
- [16] Y. Harabuchi, J. Eng, E. Gindensperger, T. Taketsugu, S. Maeda, C. Daniel, *J. Chem. Theory Comput.* **2016**, 12, 2335.
- [17] M. Fumanal, E. Gindensperger, C. Daniel, *J. Chem. Theory Comput.* **2017**, 13, 1293.
- [18] S. Mai, H. Gattuso, M. Fumanal, A. Muñoz-Losa, A. Monari, C. Daniel, L. González, *Phys. Chem. Chem. Phys.* **2017**, 19, 27240.
- [19] V. Baranovskii, D. Maltsev, *Comput. Theor. Chem.* **2014**, 1043, 71.
- [20] R. M. Carlos, M. G. Neumann, *J. Photochem. Photobiol. A* **2000**, 131, 67.
- [21] I. de Aguiar, S. D. Inglez, F. C. A. Lima, J. F.-S. Daniel, B. R. McGarvey, A. C. Tedesco, R. M. Carlos, *Inorg. Chem.* **2008**, 47, 11519.
- [22] I. de Aguiar, F. C. A. Lima, J. Ellena, V. R. S. Malta, R. M. Carlos, *Comp. Theor. Chem.* **2011**, 965, 7.
- [23] P. P. Hohenberg, W. Kohn, *Phys. Rev.* **1964**, 136, B864.
- [24] W. Kohn, L. J. Sham, *Phys. Rev.* **1965**, 140, A1133.
- [25] D. Becke, *J. Chem. Phys.* **1993**, 98, 5648.
- [26] A. Klamt, G. Schürmann, *J. Chem. Soc. Perkin Trans.* **1993**, 2, 799.
- [27] A. Klamt, *J. Phys. Chem.* **1995**, 99, 2224.
- [28] A. Klamt, V. Jonas, *J. Chem. Phys.* **1996**, 105, 9972.
- [29] P. J. Stephens, F. J. Devlin, C. F. Chabalowski, M. J. Frisch, *J. Phys. Chem.* **1994**, 98, 11623.
- [30] E. Van Lenthe, E. J. Baerends, *J. Comput. Chem.* **2003**, 24, 1142.
- [31] E. Van Lenthe, R. Van Leeuwen, E. J. Baerends, J. G. Snijders, *Int. J. Quantum Chem.* **1996**, 57, 281.
- [32] E. Runge, E. K. U. Gross, *Phys. Rev. Lett.* **1984**, 52, 997.
- [33] M. Petersilka, U. J. Gossmann, E. K. U. Gross, *Phys. Rev. Lett.* **1996**, 76, 1212.
- [34] M. J. Peach, D. J. Tozer, *J. Phys. Chem. A* **2012**, 116, 9783.
- [35] F. Wang, T. Ziegler, E. van Lenthe, S. J. A. van Gisbergen, E. J. Baerends, *J. Chem. Phys.* **2005**, 112, 204103.
- [36] F. Wang, T. Ziegler, *J. Chem. Phys.* **2005**, 113, 154102.
- [37] B. O. Roos, P. R. Taylor, P. E. M. Siegbahn, *Chem. Phys.* **1980**, 48, 157.
- [38] K. Andersson, P.-Å. Malmqvist, B. O. Roos, *J. Chem. Phys.* **1992**, 96, 1218.
- [39] J. Finley, P.-Å. Malmqvist, B. O. Roos, L. Serrano-Andrés, *Chem. Phys. Lett.* **1998**, 288, 299.
- [40] B. O. Roos, R. Lindh, P.-Å. Malmqvist, V. Veryazov, P.-O. Widmark, *J. Phys. Chem. A* **2005**, 109, 6575.
- [41] B. O. Roos, R. Lindh, P.-Å. Malmqvist, V. Veryazov, P.-O. Widmark, *J. Phys. Chem. A* **2004**, 108, 2851.
- [42] P.-O. Widmark, P.-Å. Malmqvist, B. O. Roos, *Theor. Chim. Acta* **1990**, 77, 291.
- [43] S. Miertus, E. Scrocco, J. Tomasi, *J. Chem. Phys.* **1981**, 55, 117.
- [44] E. Cancès, B. Mennucci, J. Tomasi, *J. Chem. Phys.* **1997**, 107, 3032.
- [45] G. Ghigo, B. O. Roos, P.-Å. Malmqvist, *Chem. Phys. Lett.* **2004**, 396, 142.
- [46] H. Koch, A. Sanchez de Meras, T. B. Pedersen, *J. Chem. Phys.* **2003**, 118, 9481.
- [47] N. Forsberg, P.-Å. Malmqvist, *Chem. Phys. Lett.* **1997**, 274, 196.
- [48] P.-Å. Malmqvist, B. O. Roos, B. Schimmelpfennig, *Chem. Phys. Lett.* **2002**, 357, 230.
- [49] S. Mai, F. Plasser, J. Dorn, M. Fumanal, C. Daniel, L. González, *Coord. Chem. Rev.* **2018**, 361, 74.
- [50] F. Plasser, TheoDORE, <http://theodore-qc.sourceforge.net>, **2017**.
- [51] ADF, SCM, Theoretical Chemistry, Vrije Universiteit, Amsterdam, The Netherlands, **2013** <https://www.scm.com/Downloads/>.
- [52] F. Aquilante, J. Autschbach, R. K. Carlson, L. F. Chibotaru, M. G. Delcey, L. De Vico, I. F. Galván, N. Ferré, L. M. Frutos, L. Gagliardi, M. Garavelli, A. Giussani, C. E. Hoyer, G. Li Manni, H. Lischka, D. Ma, P.-Å. Malmqvist, T. Müller, A. Nenov, M. Olivucci, T. B. Pedersen, D. Peng, F. Plasser, B. Pritchard, M. Reiher, I. Rivalta, I. Schapiro, J. Segarra-Martí, M. Stenrup, D. G. Truhlar, L. Ungur, A. Valentini, S. Vancollie, V. Veryazov, V. P. Vysotskiy, O. Weingart, F. Zapata, R. Lindh, *J. Comput. Chem.* **2016**, 37, 506.
- [53] S. Maeda, K. Morokuma, *J. Chem. Phys.* **2010**, 132, 241102.
- [54] S. Maeda, K. Ohno, K. Morokuma, *Phys. Chem. Chem. Phys.* **2013**, 15, 3683.
- [55] Y. Harabuchi, T. Taketsugu, S. Maeda, *Chem. Phys. Lett.* **2017**, 674, 141.
- [56] S. Maeda, Y. Harabuchi, Y. Ono, T. Taketsugu, K. Morokuma, *Int. J. Quantum Chem.* **2015**, 115, 258.
- [57] S. Maeda, Y. Harabuchi, M. Takagi, K. Saita, K. Suzuki, T. Ichino, Y. Sumiya, K. Sugiyama, Y. Ono, *J. Comput. Chem.* **2018**, 39, 233.
- [58] S. Maeda, Y. Harabuchi, Y. Sumiya, M. Takagi, K. Suzuki, M. Hatanaka, Y. Osada, T. Taketsugu, K. Morokuma, K. Ohno, GRRM17, [http://iqce.jp/GRRM/index\\_e.shtml](http://iqce.jp/GRRM/index_e.shtml) (accessed date 12 May **2018**).
- [59] M. J. Frisch, G. W. Trucks, H. B. Schlegel, G. E. Scuseria, M. A. Robb, J. R. Cheeseman, G. Scalmani, V. Barone, G. A. Petersson, H. Nakatsuji, X. Li, M. Caricato, A. V. Marenich, J. Bloino, B. G. Janesko, R. Gomperts, B. Mennucci, H. P. Hratchian, J. V. Ortiz, A. F. Izmaylov, J. L. Sonnenberg, D. Williams-Young, F. Ding, F. Lipparini, F. Egidi, J. Goings, B. Peng, A. Petrone, T. Henderson, D. Ranasinghe, V. G. Zakrzewski, J. Gao, N. Rega, G. Zheng, W. Liang, M. Hada, M. Ehara, K. Toyota, R. Fukuda, J. Hasegawa, M. Ishida, T. Nakajima, Y. Honda, O. Kitao, H. Nakai, T. Vreven, K. Throssell, J. A. Montgomery, Jr., J. E. Peralta, F. Ogliaro, M. J. Bearpark, J. J. Heyd, E. N. Brothers, K. N. Kudin, V. N. Staroverov, T. A. Keith, R. Kobayashi, J. Normand, K. Raghavachari, A. P. Rendell, J. C. Burant, S. S. Iyengar, J. Tomasi, M. Cossi, J. M. Millam, M. Klene, C. Adamo, R. Cammi, J. W. Ochterski, R. L. Martin, K. Morokuma, O. Farkas, J. B. Foresman, D. J. Fox, Gaussian 16 (Revision A.03), Gaussian, Inc., Wallingford, CT, **2016**.
- [60] W. B. Connick, A. J. Di Bilio, M. G. Hill, J. R. Winkler, H. B. Gray, *Inorg. Chim. Acta* **1995**, 240, 169.
- [61] H. Brahim, C. Daniel, *Comp. Theor. Chem.* **2014**, 15, 219.
- [62] S. Finck, J. T. Issenhuth, S. Despax, C. Sirlin, M. Pfeffer, C. Poidevin, C. Gourlaouen, A. Boeglin, C. Daniel, *J. Organomet. Chem.* **2013**, 760, 248.
- [63] S. Villaume, A. Strich, C. Daniel, S. A. Perera, R. J. Bartlett, *Phys. Chem. Chem. Phys.* **2007**, 9, 6115.
- [64] D. Ambrosek, S. Villaume, L. González, C. Daniel, *Chem. Phys. Lett.* **2006**, 417, 545.
- [65] N. Ben Amor, S. Villaume, D. Maynau, C. Daniel, *Chem. Phys. Lett.* **2006**, 421, 378.
- [66] J. Jimenez, I. Chakraborty, A. Dominguez, J. Martinez-Gonzalez, W. M. C. Sameera, P. K. Mascharak, *Inorg. Chem.* **2018**, 57, 1766.

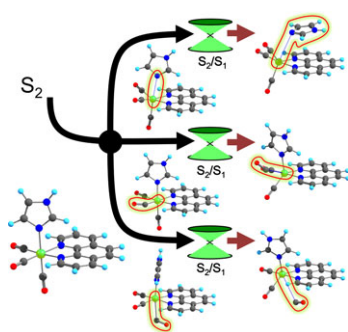
Received: 31 May 2018

Revised: 25 June 2018

Accepted: 26 June 2018

Published online on 00 Month 2018

SGML and CITI Use Only  
DO NOT PRINT



The structural exploration of the potential energy surfaces associated to the low-lying singlet excited states of a manganese carbonyl imidazole-substituted  $\alpha$ -diimine complex, potentially functional PhotoCORM under visible irradiation, highlights the active reactive channels of dissociation. Qualitative state correlation diagrams that connect the low-lying excited states of the parent molecule to those of the fragments  $[\text{Mn}(\text{imidazole})(\text{CO})_2(\text{phen})]^+ + \text{CO}_{\text{ax}}$  and  $[\text{M}(\text{CO})_3(\text{phen})]^+ + \text{Imidazole}$  point to two dissociative channels. The two lowest  $S_1$  and  $S_2$  singlet states are weakly dissociative for the CO loss with energy barriers generated nearby the FC region. Systematic searches for critical geometries identify several dissociative pathways, namely, equatorial CO bent, imidazole dissociation, or axial CO bent are competitive with the direct CO loss.

Uncorrected Proofs

58  
59  
60  
61  
62  
63  
64  
65  
66  
67  
68  
69  
70  
71  
72  
73  
74  
75  
76  
77  
78  
79  
80  
81  
82  
83  
84  
85  
86  
87  
88  
89  
90  
91  
92  
93  
94  
95  
96  
97  
98  
99  
100  
101  
102  
103  
104  
105  
106  
107  
108  
109  
110  
111  
112  
113  
114

OS

1  
2  
3  
4  
5  
6  
7  
8  
9  
10  
11  
12  
13  
14  
15  
16  
17  
18  
19  
20  
21  
22  
23  
24  
25  
26  
27  
28  
29  
30  
31  
32  
33  
34  
35  
36  
37  
38  
39  
40  
41  
42  
43  
44  
45  
46  
47  
48  
49  
50  
51  
52  
53  
54  
55  
56  
57